

Spectroscopy and Imaging Performance of the Liquid Xenon Gamma-Ray Imaging Telescope (LXeGRIT)

E. Aprile^a, A. Curioni^a, V. Egorov^a, K.-L. Giboni^a, U.G. Oberlack^a,
S. Ventura^{a,b}, T. Doke^c, J. Kikuchi^c, K. Takizawa^c,
E.L. Chupp^d, P.P. Dunphy^d

^aColumbia Astrophysics Laboratory, Columbia University

^bINFN–Padova, Italy

^cWaseda University, Japan

^dUniversity of New Hampshire, USA

ABSTRACT

LXeGRIT is a balloon-borne Compton telescope based on a liquid xenon time projection chamber (LXeTPC) for imaging cosmic γ -rays in the energy band of 0.2–20 MeV. The detector, with 400 cm² area and 7 cm drift gap, is filled with high purity LXe. Both ionization and scintillation light signals are detected to measure the energy deposits and the three spatial coordinates of individual γ -ray interactions within the sensitive volume. The TPC has been characterized with repeated measurements of its spectral and Compton imaging response to γ -rays from radioactive sources such as ²²Na, ¹³⁷Cs, ⁸⁸Y and Am-Be. The detector shows a linear response to γ -rays in the energy range 511 keV–4.4 MeV, with an energy resolution (FWHM) of $\Delta E/E = 8.8\% \sqrt{1\text{MeV}/E}$. Compton imaging of ⁸⁸Y γ -ray events with two detected interactions is consistent with an angular resolution of ~ 3 degrees (RMS) at 1.8 MeV.

Keywords: gamma-rays, instrumentation, imaging, telescope, balloon missions, high energy astrophysics

1. INTRODUCTION

Progress in MeV γ -ray astrophysics has lagged far behind that in the X-ray band and at high energies, because of the difficulty of imaging MeV photons combined with the high background and the low cosmic source fluxes. Results from CGRO–COMPTEL,¹ the only Compton Telescope in space to-date, have shown both the promise and the challenges of this field. To explore the rich scientific potential of this energy band, new instruments are needed which combine substantially higher detection efficiency and background rejection capabilities, within a large field-of-view.

The development of a liquid xenon time projection chamber (LXeTPC) at Columbia was initiated to demonstrate the feasibility of the technique and to study its capability as efficient Compton telescope for MeV γ -ray astrophysics. The combination of calorimetry and 3D event imaging in a TPC is especially powerful for reconstructing the multiple Compton histories of MeV γ -rays, and thus the incoming direction and energy on an event-by-event basis. Equally important, the imaging capability proves to be a powerful tool in rejecting background. After the characterization in the laboratory, the LXeTPC has been turned into a balloon-borne instrument (LXeGRIT) to test its performance in the near space environment. A description of the instrument and its performance during its May 1999 balloon flight in New Mexico are reported elsewhere in these proceedings.² Here we present some of the results on the detector spectral and imaging performance, obtained during the pre-flight calibration experiments with radioactive sources of gamma-rays at energies between 511 keV and 4.4 MeV.

2. THE LXETPC AS γ -RAY SPECTROMETER AND COMPTON IMAGER

A schematic of the LXeTPC and its principle of operation is shown in Fig. 1. The TPC is assembled in a cylindrical vessel of 10 l volume, filled with high purity LXe at a temperature of $\sim -100^\circ$ C. The sensitive area is 20×20 cm² and the maximum drift length is 7 cm. The detector operates over a wide energy range from ~ 200 keV to 20 MeV.

Send correspondence to: E. Aprile, Columbia University, Astrophysics Laboratory, 550 West 120th Street, New York, NY 10027

E-mail: age@astro.columbia.edu

LXeGRIT Web page: <http://www.astro.columbia.edu/~lxe/lxegrit/>

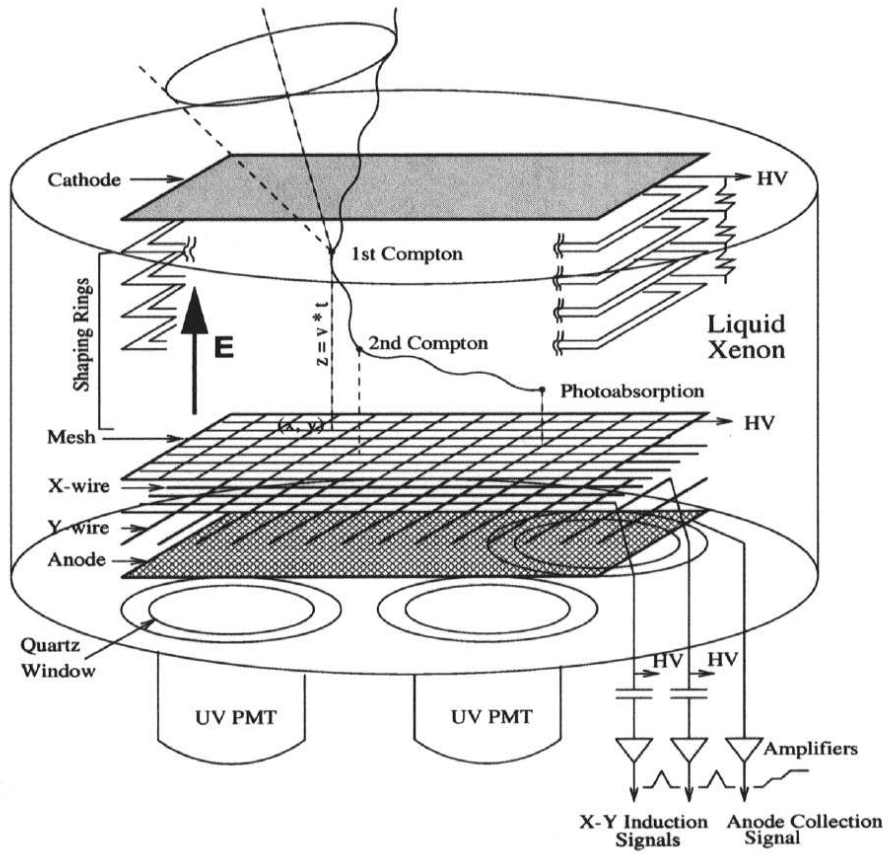


Figure 1. LXeTPC schematic.

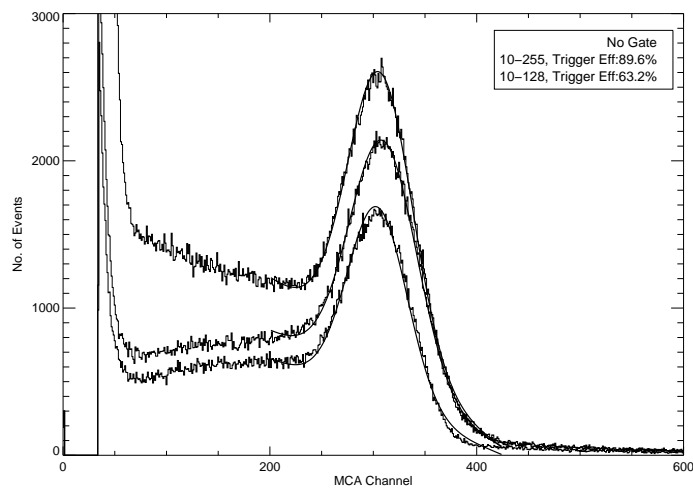


Figure 2. ^{137}Cs 662 keV energy spectra for all anode signals (*upper curve*) and for anode signals with a light trigger (*lower curves*) for two discriminator windows.

2.1. Light signals detection and processing

Both ionization and scintillation light signals, produced by a charged particle in the liquid, are detected to measure its energy and 3D position. The fast (< 5 ns) Xe light (175 nm), detected by four UV sensitive photomultiplier tubes (PMTs) coupled to the detector vessel by quartz windows, provides the event trigger. The signals from the PMTs are passed through a set of window discriminators: the lower threshold of the discriminators avoids triggering the readout on noise pulses, while the upper threshold reduces the number of high-energy charged particle events. The choice of the upper and lower threshold, together with the PMTs high-voltage, impacts significantly the detector's trigger efficiency.

The light level seen by the PMTs is extremely low. The total number of photons produced in LXe by a charged particle is reduced by the quenching of the recombination luminescence due to the applied electric field. More photons are lost due to geometrical effects (solid angle), low reflectivity of the chamber materials, optical transmission of the wires and anode meshes and transmittance by the quartz windows. The efficiency of each PMT was estimated by measuring the count rate of the triggering events relative to the total count rate. This was done by comparing the Multi Channel Analyser (MCA) spectrum of the charge signals from the anode directly above the PMT, gated by the PMT light trigger and ungated. The ratio of events with a trigger and of all events, under the full energy peak, was taken as the trigger efficiency for the particular γ -ray energy line. Three spectra for a collimated ^{137}Cs source, placed above the center of one anode, are shown in Fig. 2. The voltage on the corresponding PMT was 1800 V. The MCA spectra were taken with $10 \mu\text{s}$ shaping time for the anode shaping amplifier. Given the $35 \mu\text{s}$ maximum drift time, γ -rays interacting two or more times in locations more than $10 \mu\text{s}$ apart in drift time contribute to the background below the line. From a fit of the lines, the trigger efficiency at 662 keV is 89.6 % for the discriminator window of 10–255. By lowering the upper threshold from 255 to 128, the efficiency drops to 63 %.

2.2. Charge signals detection and processing

The drift of free ionization electrons in the LXeTPC uniform electric field, typically 1 kV/cm, induces charge signals on a pair of orthogonal planes of parallel wires with a 3 mm pitch, before collection on four independent anodes (see Fig. 1). Each of the 62 X-wires and 62 Y-wires and each anode is amplified and digitized at a sampling rate of 5 MHz, to record the pulse shape. The X-Y coordinate information is obtained from the pattern of hits on the wires, while the energy is obtained from the amplitude of the anode signals. The Z-coordinate is determined from the drift time measurement, referred to the light trigger. For a review of the TPC signal characteristics and their electronics readout we refer to Aprile et al. 1998.⁴ The system is such that the equivalent noise charge on the wires is typically less than $\sim 400 e^-$ RMS, while the noise on the anodes, of higher capacitance, is $\sim 800 e^-$ RMS. With these noise conditions, the TPC can well detect the multiple interactions of MeV γ -rays, with a minimum energy deposit of ~ 150 keV.

Fig. 3 shows the TPC display of a ^{88}Y 1.8 MeV γ -ray event. The digitized signals on all wires and active anodes are shown as a function of drift time. The incoming photon makes two Compton scatterings before being photoabsorbed. In this “3-steps” event, in fact, the sum of the three anode pulse heights gives 1.8 MeV. The corresponding location of the interactions are clearly seen on the X-Y wires. An efficient and fast signal recognition algorithm has been developed to sort the different event topologies and to obtain the energy and X-Y-Z coordinates from the digitized signals of each interaction recorded in the sensitive volume.³ With this information, and with the gain and energy calibration curves, spectral and imaging analysis of gamma-ray sources is then carried out.

2.3. Energy Resolution and Calibration

The response of the TPC to γ -rays was characterized in several experiments with the electronics, trigger conditions and data acquisition system as used during the May 99 flight. The following radioactive sources were used: ^{137}Cs , ^{22}Na and ^{88}Y with lines at 662 keV, 511 keV and 1275 keV, 898 keV and 1836 keV, respectively. The sources were either collimated or placed at some distance (2–4 meters) from the TPC. Data were also taken with an Am-Be neutron source, which emits 4.43 MeV gamma-rays, as well as with cosmic rays.

For detectors with a large drift region like LXeGRIT, the Xe purity largely determines the charge yield and thus the spectral response. To minimize the charge loss due to attachment of free electrons to electro-negative impurities, an efficient purification system was developed and has been fully discussed in Xu 1998.⁶ The simple relation

$$Q_{det} = Q_0 \cdot \exp\left(-\frac{z}{\lambda_{att}}\right) \quad (1)$$

describes the detected charge Q_{det} , given an initial charge Q_0 at a distance z from the collection point. The parameter λ_{att} is the attenuation length for electrons drifting in liquid Xe. If not corrected, even a modest (few percent) dependence of the collected charge on z would deteriorate the energy resolution.

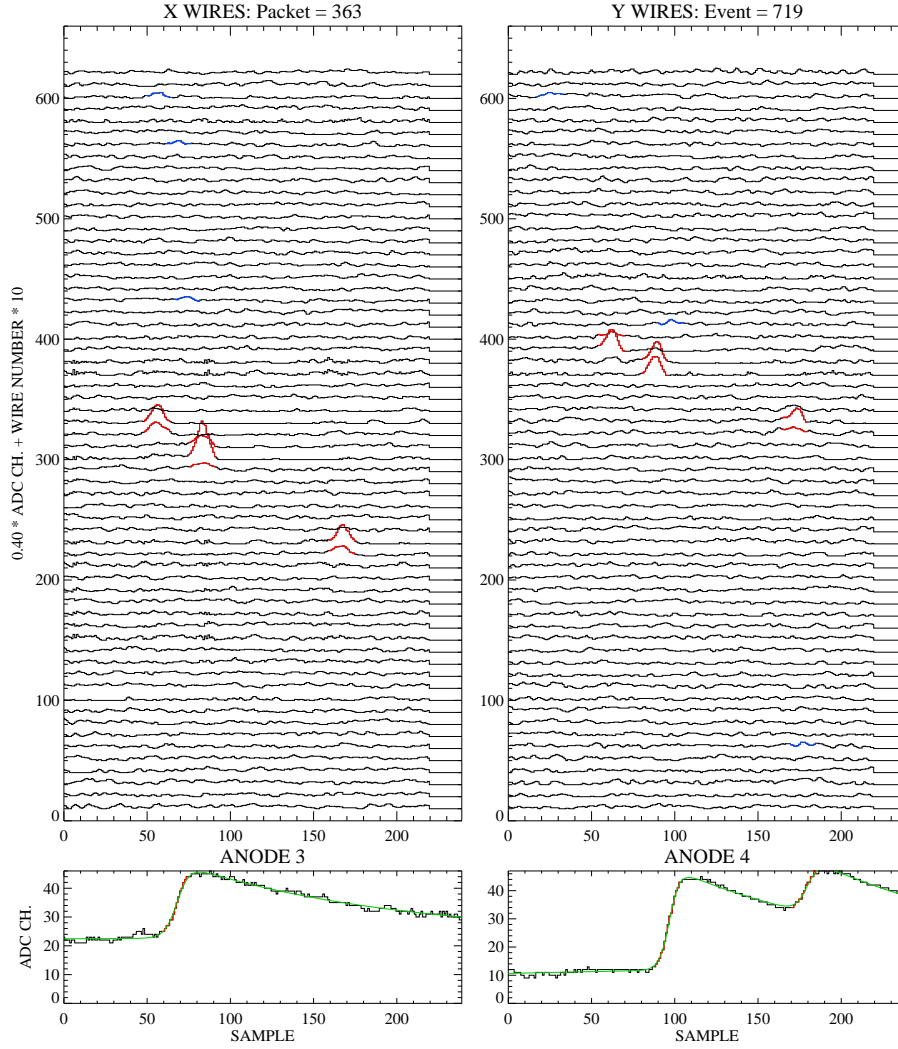


Figure 3. LXeGRIT on-line display of a 1.8 MeV γ -ray event with multiple Compton interactions.

The measurement of the absolute depth of an interaction in the light triggered LXeTPC offers a direct method to infer the drifting electron lifetime and thus the purity of the LXe. Given a γ -ray line, in this case 662 keV, the procedure consists in measuring the photopeak amplitude for different z (i.e. drift time) slices, as shown in Fig. 4. The photopeak dependence *vs.* z is then fitted with the relation 1 to yield λ_{att} , i.e. the electron lifetime. The scatter plot of the amplitude of the ^{137}Cs events *vs.* drift time at 1 kV/cm is shown in Fig. 5, for single interaction events. The enhancement seen in correspondence to the 662 keV full energy peak moves to lower pulse heights for longer drift time. The measured drifting electron lifetime is about 360 μs : this lifetime corresponds to an attenuation length of 80 cm, to be compared with the 7 cm maximum drift length in our detector. A correction for attachment to impurities is applied during event reconstruction on an event-by-event basis, removing the dependence of the signal amplitude on the distance from the anode and so significantly improving the spectral performance.

The spectral performance of the LXeTPC, inferred from the analysis of either single or multiple interaction events, is shown with the reconstructed energy spectra of the ^{22}Na , ^{137}Cs , ^{88}Y and Am-Be sources (see Figs. 6, 7, 8, 9).

Fig. 6 shows the 511 keV energy spectrum measured with a tagged ^{22}Na source: ^{22}Na simultaneously emits a 1275 keV γ -ray plus a positron, promptly annihilating and producing two 511 keV γ -rays in opposite directions, so that one of the two 511 keV photons can be used to tag the other one, reducing 1275 keV and pile-up events. In our case, when 511 keV energy deposit was detected in a NaI(Tl) scintillation counter placed above the TPC, a trigger was sent to the TPC.

Fig. 7 shows the energy spectrum of a collimated ^{137}Cs source. In both cases, we point out the large enhancement of the *peak-to-Compton-ratio* obtained with multiple interactions events, compared to the single interaction events spectrum.

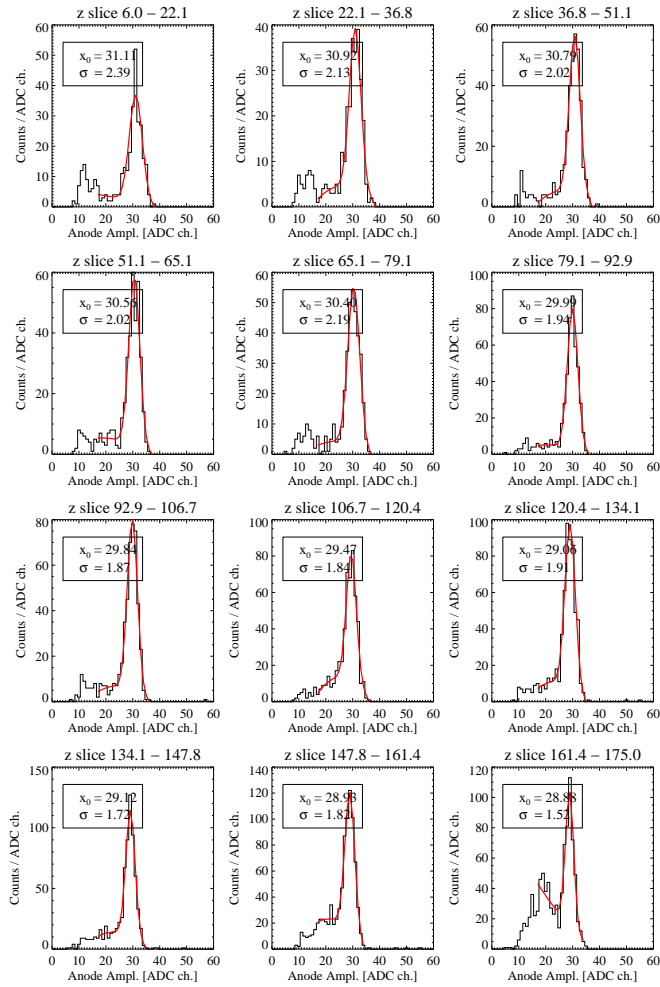


Figure 4. ^{137}Cs (collimated source) energy spectra for different drift times: each “slice” of the fiducial volume is 6 mm thick. Going from top to bottom the drift time increases.

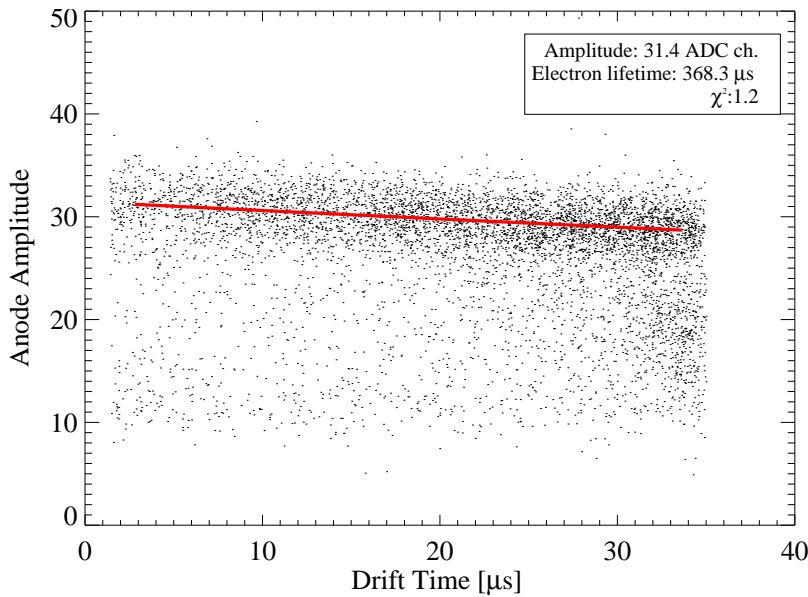


Figure 5. Anode amplitude (ADC ch.) vs. drift-time (μs). Drift-time is directly converted in z -position. The solid line is the result of an exponential fit to the photopeak position for various slices in drift time.

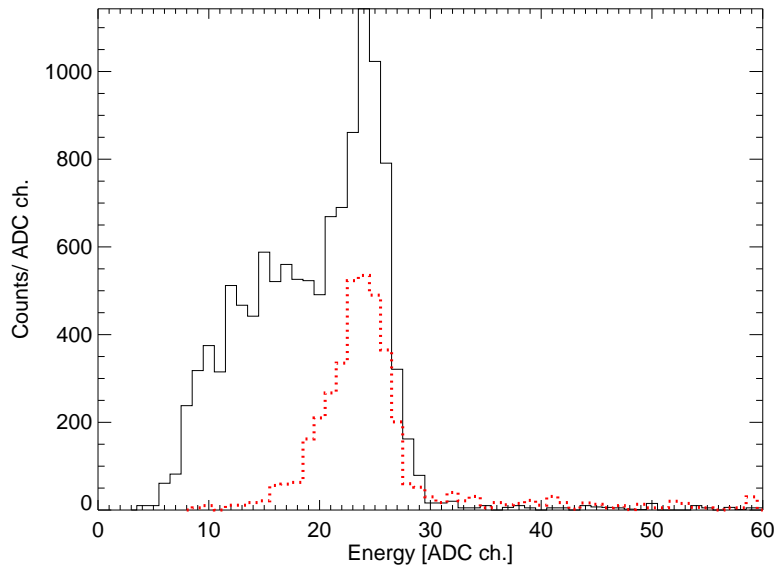


Figure 6. ^{22}Na 511 keV energy spectrum for single interaction (*solid line*) and Compton interaction events (*dotted line*). Note the suppression of the Compton continuum and the large enhancement of the peak-to-Compton ratio in the multiple interactions sample.

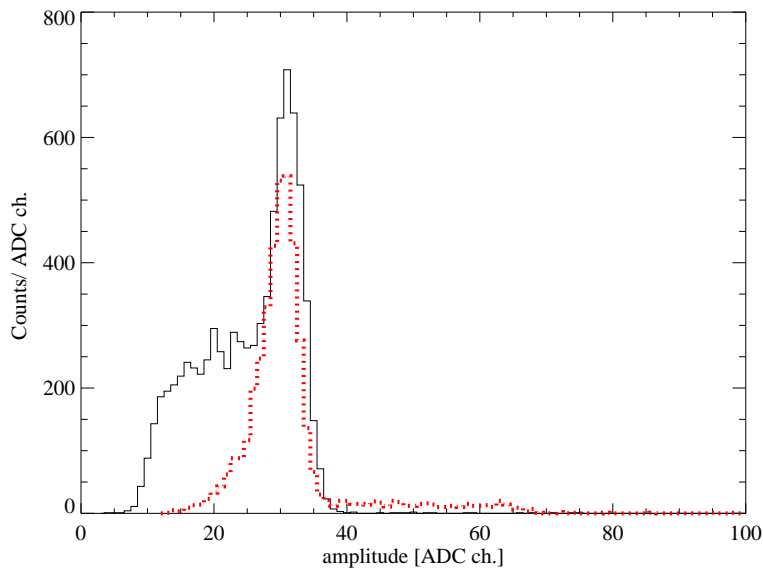


Figure 7. ^{137}Cs 662 keV energy spectrum for single interaction (*solid line*) and Compton interaction events (*dotted line*). Note the suppression of the Compton continuum and the large enhancement of the peak-to-Compton ratio in the multiple interactions sample.

Fig. 8 shows the ^{88}Y energy spectrum obtained from events with two interactions (“2-step” events). In this experiment the source was placed about 2 m above the TPC to simulate a parallel γ -rays beam for imaging analysis, as discussed in the next section. Aside the 898 and 1836 keV photopeaks, the single escape peak (1325 keV) for 1836 keV photons is detected. Fig. 9 shows the energy spectrum from an Am-Be neutron source. Again “2-step” events were used. Since the cross-section for pair-production is large at 4.4 MeV, the single escape peak (3.92 MeV) is prominent. Photopeak, single and double (detected in the “1-step” events spectrum, not shown here) escape peaks and the Compton edge have been used in the energy calibration.

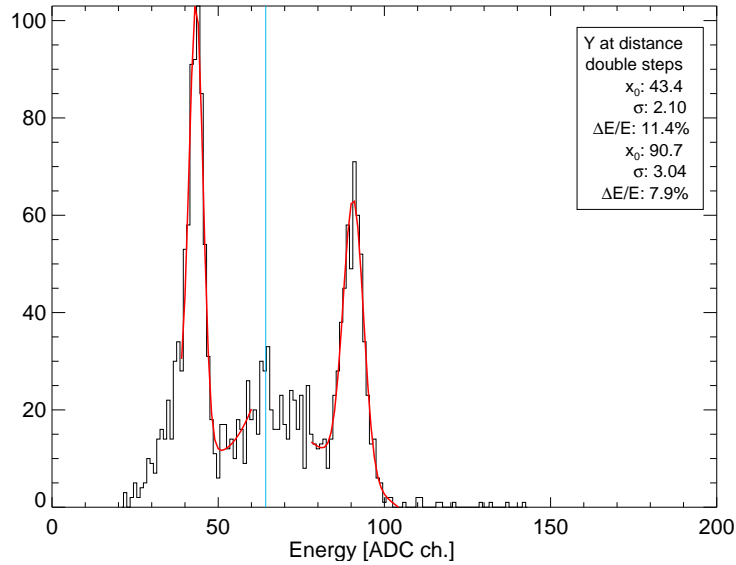


Figure 8. ^{88}Y 898 keV and 1836 keV energy spectrum for two interaction (“2–step”) events. The source was placed about 2 m above the TPC.

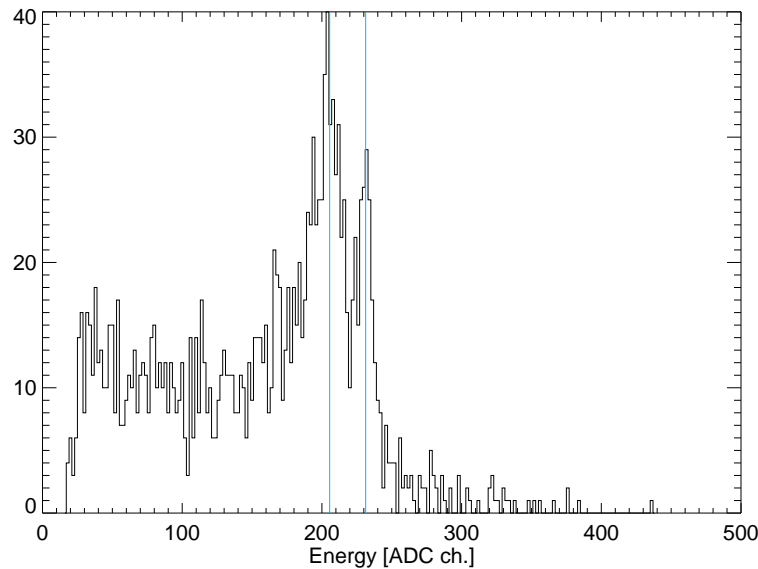


Figure 9. Am-Be energy spectrum for two interaction (“2–step”) events. The photopeak (4.43 MeV) and the single escape peak (3.92 MeV) are clearly identified.

The calibration curve obtained combining the ^{137}Cs , ^{22}Na , ^{88}Y and Am-Be data is shown in Fig. 10. The non linear term is small, indicating good proportionality over the energy range 511 keV– 4.43 MeV. The energy resolution of all the lines is consistent with a value of 10 % (FWHM at 1 MeV), scaling as $1/\sqrt{E}$. This value includes electronics noise, shielding inefficiency and non linearities in the gain response due to the electronics as well as the signal processing analysis. The noise subtracted energy resolution is 8.8 % (FWHM at 1 MeV) (see Fig. 11), in excellent agreement with expectations.

2.4. Compton Imaging and Angular Resolution

To test the Compton imaging performance of the telescope, the LXeTPC was irradiated with a parallel beam of γ -rays from a ^{88}Y calibration source placed at a distance of several meters. Here we present the results obtained with γ -ray events, for which two interactions are recognized in the sensitive LXe volume (“2–step” events). Events with a single

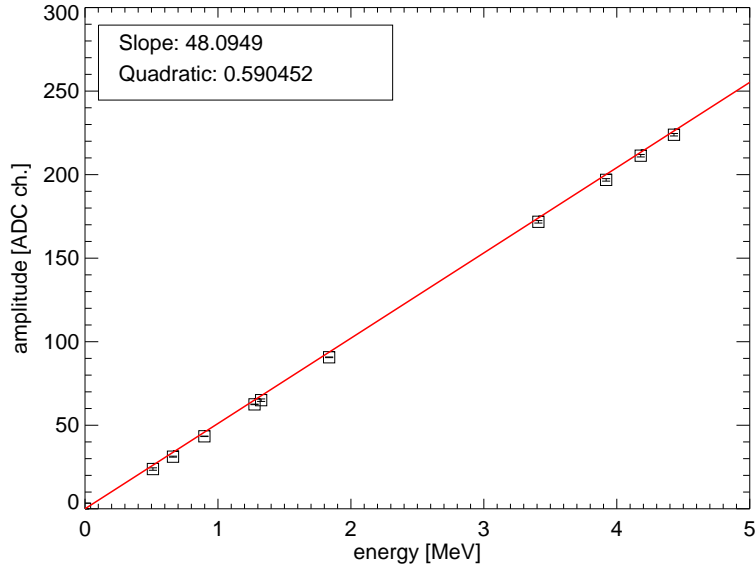


Figure 10. Energy calibration curve for one of the four LXeTPC anodes: anode amplitude vs. energy fitted with $amp = b \cdot E + c \cdot E^2$. In the inlet, $b =$ “slope” and $c =$ “quadratic”.

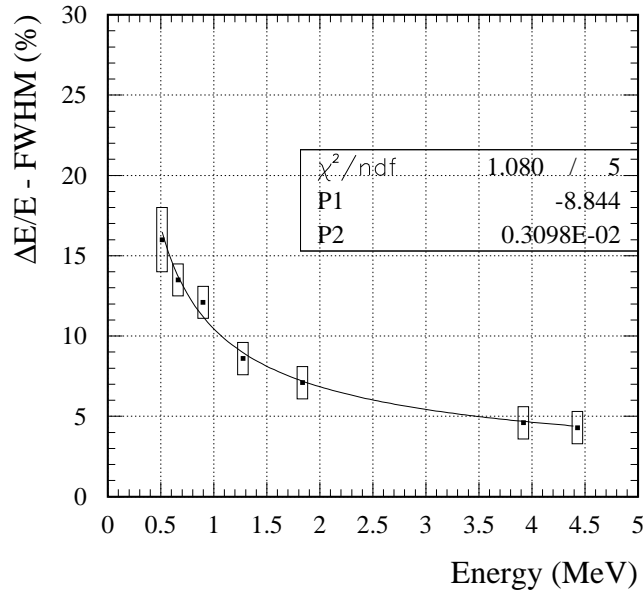


Figure 11. Energy resolution vs. energy: $\Delta E_{\text{LXe}}/E = 8.8\% \sqrt{1\text{MeV}/E}$

Compton scattering followed by a photoabsorption are the simplest ones that can be used for imaging a source at a known location. The process of determining the imaging response breaks down into three parts:

1. Energy calibration, which is necessary for the relation of charge deposits to the electron mass m_0c^2 in the calculation of the Compton scatter angle $\bar{\phi}$ (equation 3). This includes correction for charge losses due to electron attachment according to the depth of the interaction (z-position), as described in section 2.3. The conversion from ADC counts

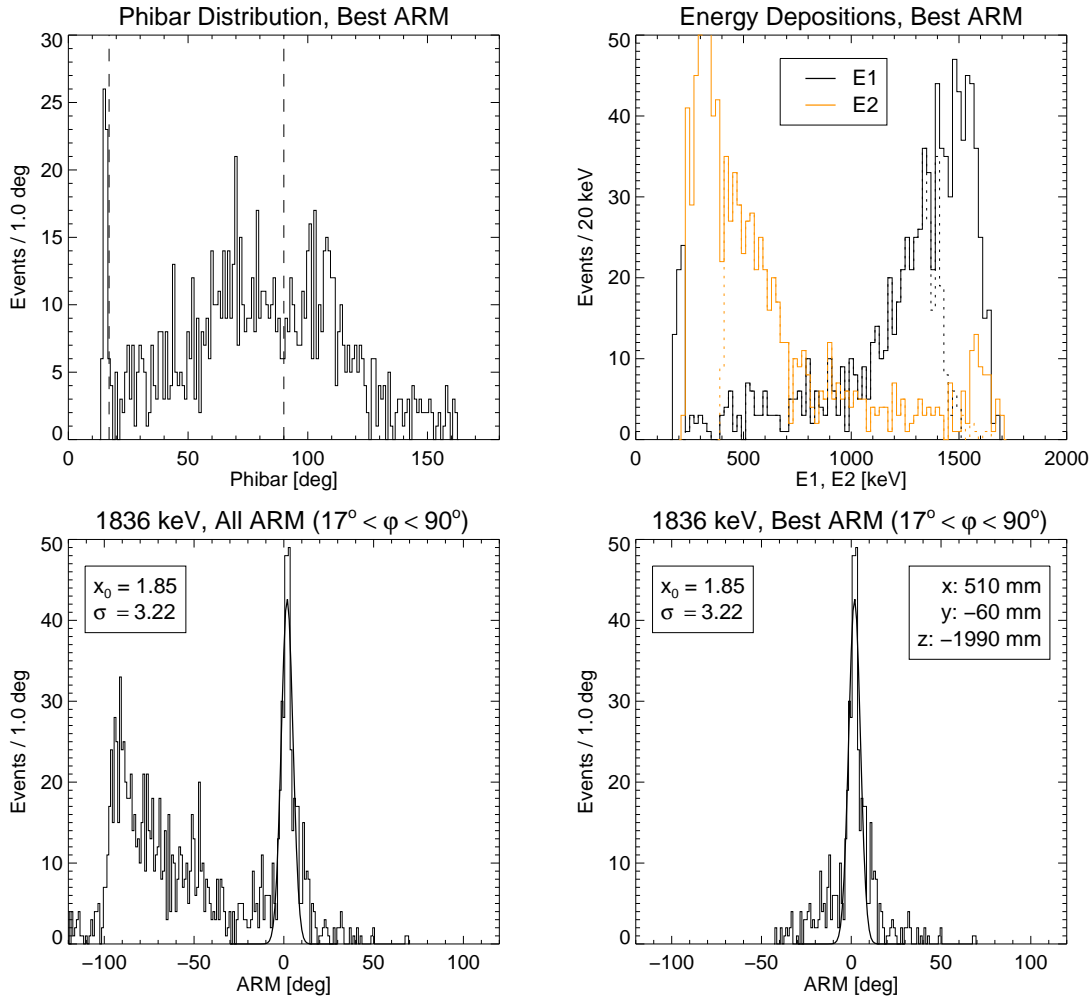


Figure 12. *Top left:* $\bar{\phi}$ distribution for two-step events in the full energy peak of the 1836 keV ^{88}Y line. *Top right:* energy deposit in each interaction. *Bottom:* ARM spectra for two-step events in the full energy peak of the 1836 keV ^{88}Y line.

to keV is then based on the four anode calibration curves, such as that of Fig. 10.

2. Determination of the time sequence of the two interactions. For events with two interactions, the LXeTPC provides no redundant measurement that would uniquely determine the interactions sequence. In the case of calibration data with known source position, the sequence with the minimum value of “angular resolution measure” (ARM) as defined below, can be chosen. For data with unknown source location, the decision on the correct sequence can be based on a maximum energy value assigned to the second step, since the photo-absorption cross section falls off steeply beyond 200 keV in xenon (see^{7,8} for similar approaches). Alternatively, both sequences might be used in a likelihood analysis, which uses relative probabilities for each sequence with respect to a source position. Such extended instrumental response would be derived from Monte Carlo simulations.
3. Derivation of the ARM distribution, i.e., the distribution of scatter angles $\bar{\phi}$ derived from Compton kinematics minus the geometrical scatter angles ϕ^\triangleleft between the known source position and the measured scatter direction, given by the two interaction locations:

$$ARM = \bar{\phi} - \phi^\triangleleft \quad (2)$$

$$\cos \bar{\phi}_{ij} = 1 - \frac{m_0 c^2}{E_j} + \frac{m_0 c^2}{E_i + E_j} \quad i, j = \{1, 2\} \text{ or } \{2, 1\} \quad (3)$$

$$\cos\phi_{ij}^{\triangleleft} = \frac{\vec{r}_{ij} \cdot \vec{r}_{*i}}{|\vec{r}_{ij}| |\vec{r}_{*i}|} \quad (4)$$

E_i, E_j denote the energy deposits presumed to be first and second, respectively. $\vec{r}_{ij} = \vec{r}_j - \vec{r}_i$ is the vector between the locations i, j and \vec{r}_{*i} is the vector between the source and location i .

For a γ -ray line source, as is the case for our calibration data, events can be restricted to the full-energy peak, i.e., amplitudes $A_1 + A_2 \approx A_{\text{line}} \pm 2\sigma$. The ^{88}Y energy spectrum with the two lines at 898 keV or 1836 keV as obtained from two-step events was previously shown in Fig. 8. Also, we require $\cos\bar{\phi} \geq -1$ for a valid Compton sequence. Invalid sequences can result in $\cos\bar{\phi}$ values < -1 . In fact, true Compton sequences with large scatter angles, can also yield $\cos\bar{\phi}$ values < -1 , due to the energy uncertainty of the measurement. Back-scattered events would be rejected in any case since they provide a poor imaging response. Results from the analysis of 1836 keV “2-step events” from ^{88}Y at a distance of about 2 m and at a zenith angle of $\sim 25^\circ$ are shown in Fig. 12. The *Top left* panel shows the $\bar{\phi}$ distribution for events in the full energy peak. The *Top right* panel shows the distribution of the energy deposit in each interaction. The *Bottom left* panel shows the ARM distribution of the events in the full energy peak, derived without selecting a time sequence, while the sequences with the smaller ARM value for a given source position was selected for the *Bottom right* panel. The ARM values for the two sequences are sufficiently separated, with the false sequence assuming a maximum around -93° , such that choosing the smaller ARM, in the *Bottom right* figure, does not bias the ARM peak for the correct sequence. The imaging response for these two-step events consists of a narrow peak of 3.3° (1σ) for a scatter angle selection of $17^\circ < \bar{\phi} < 90^\circ$. This angular resolution value is consistent with expectations, as shown in Fig. 13: for a scatter angle of 70° the resolution is about 7° (FWHM) at 1.8 MeV. The expected LXeGRIT angular resolution for a γ -ray line at 1.8 MeV shown in this figure was calculated based on the experimental energy resolution (FWHM) of $\Delta E/E = 10\% \sqrt{1\text{MeV}/E}$ and assuming a 2° geometrical angle contribution due to the uncertainty in the position measurement.

The non-Gaussian wings in the measured ARM distribution may be due to three-interaction events that are seen as two steps within the resolution of the detector, or to imperfections in the off-line fitting of the anode waveform. Note that with a minimum spatial separation of ~ 2 cm between the two interactions, the angular response is fully determined by the energy resolution and by the lowest energy threshold, which in this data set was about 170 keV. This imposes an energy-dependent lower threshold in $\bar{\phi}$. For events with three or more interactions, the correct sequence of scatterings can be inferred from the redundant position and energy information measured by the TPC for each interaction. The performance of a Compton sequence reconstruction algorithm on LXeGRIT “3-step” events is reported in Oberlack et al. 2000.⁹ In this paper we show that the ARM distribution for the 1836 keV line of ^{88}Y events has a width of $\sim 3^\circ$ (1σ), consistent with the result obtained with the “2-step” events.

3. CONCLUSIONS

During 1999 the spectral and imaging performance of the LXeGRIT instrument was extensively measured with a variety of γ -ray sources, spanning the energy range 511 keV–4.4 MeV, in preparation for the May ’99 balloon flight. Results can be summarized as follows:

- the LXeTPC energy response shows a good linearity over the measured. energy range

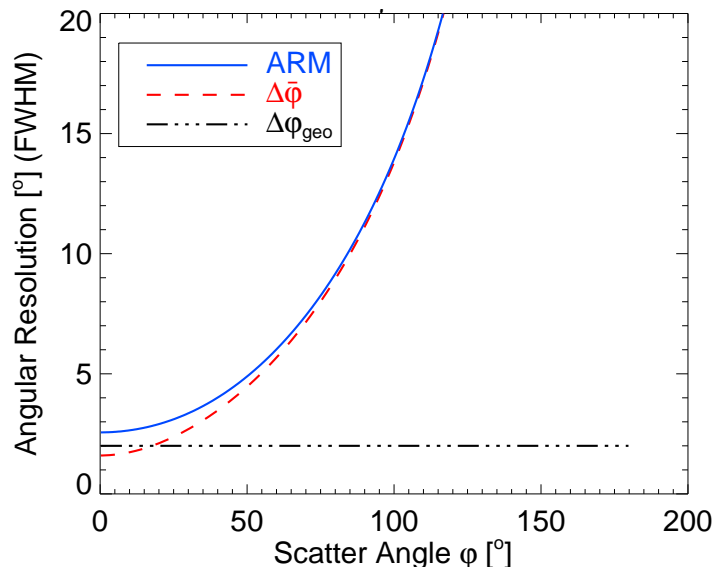


Figure 13. Angular resolution (ARM) vs. $\bar{\phi}$ for 1.8 MeV photons (solid line) and contributions from energy resolution (dashed line) and position resolution (dash-dotted line).

- the LXeTPC energy resolution, at an electric field of 1kV/cm, is 8.8% FWHM at 1 MeV scaling with $1/\sqrt{E}$. This value is consistent with previous results, obtained however with simple gridded ionization chambers with drift regions of a few mm to a few cm (see for example Aprile et al. 1991¹⁰).
- the 3D imaging capability of the TPC has been confirmed as a powerful tool to suppress background events and to enhance the *peak-to-Compton ratio* in the measured spectral distributions.
- the TPC works as a Compton telescope: γ -ray sources can be imaged with an angular resolution consistent with expectations (3° RMS for 1.8 MeV γ -rays).
- the overall performance of the TPC in the laboratory shows excellent stability in time, from the liquid purity to the high voltage, from the cryogenics to the analog and digital electronics.

These results confirm the applicability of this new detector concept to MeV γ -ray astrophysics.

ACKNOWLEDGMENTS

This work was supported by NASA under grant NAG5-5108.

REFERENCES

1. Schönfelder V., et al., 1993, ApS 86, 657
2. Aprile E., et al., 2000, SPIE Conference Proceedings, Vol. No. 4140
3. Oberlack U.G. et al., in preparation
4. Aprile E., et al., 1998. NIM A 412, 425
5. Aprile E., et al., AIP Conference Proceedings, No. 510, p. 799, 2000
6. Xu F., Ph.D. Dissertation Thesis, Columbia University, 1998
7. Boggs, S. E. and Jean, P., 2000, A&AS, in press (astro-ph/0005250)
8. Schmid, G. J., et al., 1999, NIM A 430, 69
9. Oberlack U.G. et al., 2000, SPIE Conference Proceedings, Vol. No. 4141
10. Aprile E., et al., 1991. NIM A 302, 177